Journal of Fluids and Structures (1998) **12,** 475–489
Article No. fl970149

MEASUREMENT OF STEADY AND UNSTEADY HYDRODYNAMIC LOADS ON A NUCLEAR FUEL BUNDLE

B. A. W. Smith and D. D. Derksen

Atomic Energy of Canada Limited, Chalk River Laboratories
Chalk River, Ont. Canada K0J 1J0

(Received 12 May 1997 and in revised form 28 January 1998)

A test rig was developed to measure the steady and unsteady hydrodynamic loads on a nuclear fuel bundle, as part of an investigation of wear in the fuel channels of pressurized heavy-water nuclear reactors. This paper describes the design, calibration, and operation of the test rig. Steady and unsteady forces are presented for two fuel channel inlet hardware configurations. The results show that adding a flow straightener to the inlet hardware eliminated forces caused by an upstream flow instability and reduced broad-band turbulent forces.

1. INTRODUCTION

1.1. General Introduction

in 1993, a program was established to investigate the mechanisms that caused damage to a number of fuel bundles and pressure tubes in the Bruce and Darlington CANDU nuclear reactors. The objective of this program is to develop sufficient understanding of the damage mechanism to determine ways to minimize damage in existing reactors and avoid it in future reactors. As part of this program, a test rig was developed to characterize the forces acting on the inlet fuel bundle. This bundle load measurement (BLM) rig was used to measure the steady and unsteady hydrodynamic loads on a fuel bundle in a room-temperature test rig. This paper describes the design, calibration, and operation of the BLM rig. Test results for the original and modified fuel channel hardware are presented. Other work has been performed to determine the dynamic response of the fuel and to determine the damage related to this response. To allow the reader to appreciate the motivation for this work, a brief description of the CANDU reactor is first presented.

In CANDU pressurized heavy-water reactors, the natural uranium dioxide fuel is housed in fuel bundles like that shown in Figure 1. Each fuel bundle consists of a cluster of 37 parallel cylindrical tubes, called fuel elements, filled with fuel pellets. The bundles are approximately 0.1 m in diameter and 0.5 m in length. Bearing pads are located along the outside of the bundle to prevent the fuel element sheaths from contacting the pressure tube.

CANDU reactors have many horizontal fuel channels passing through the reactor core. As shown in Figure 2, a fuel channel consists of a pressure tube with end-fittings and a calandria tube. The calandria tube surrounds the pressure tube in the reactor core. Twelve

0889–9746/98/040475 + 15 $30.00

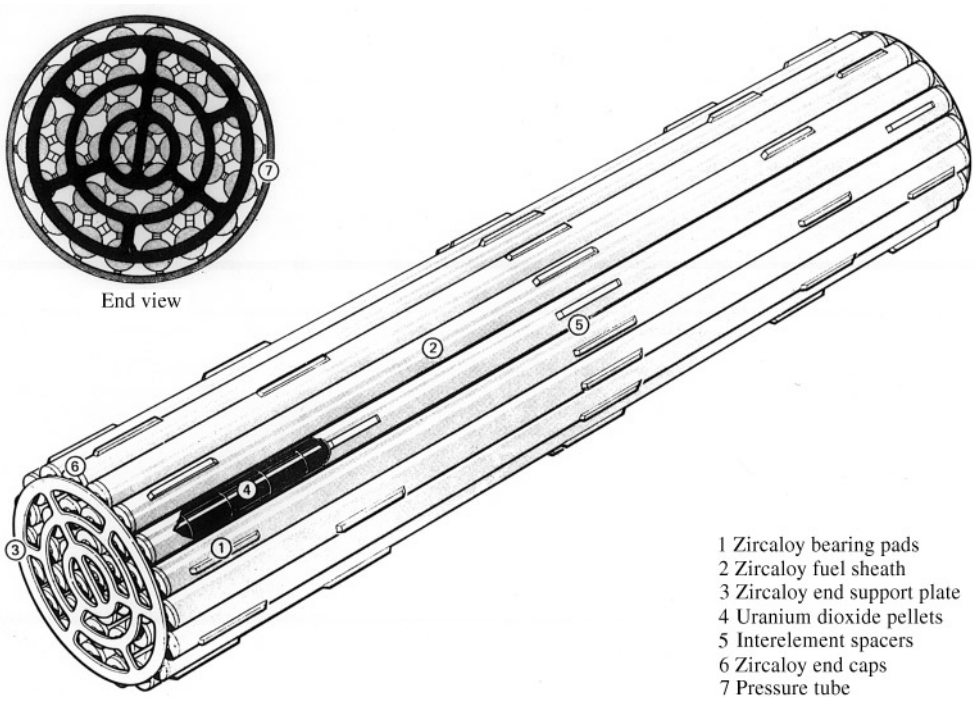

Figure 1. Bruce-type CANDU fuel bundle.

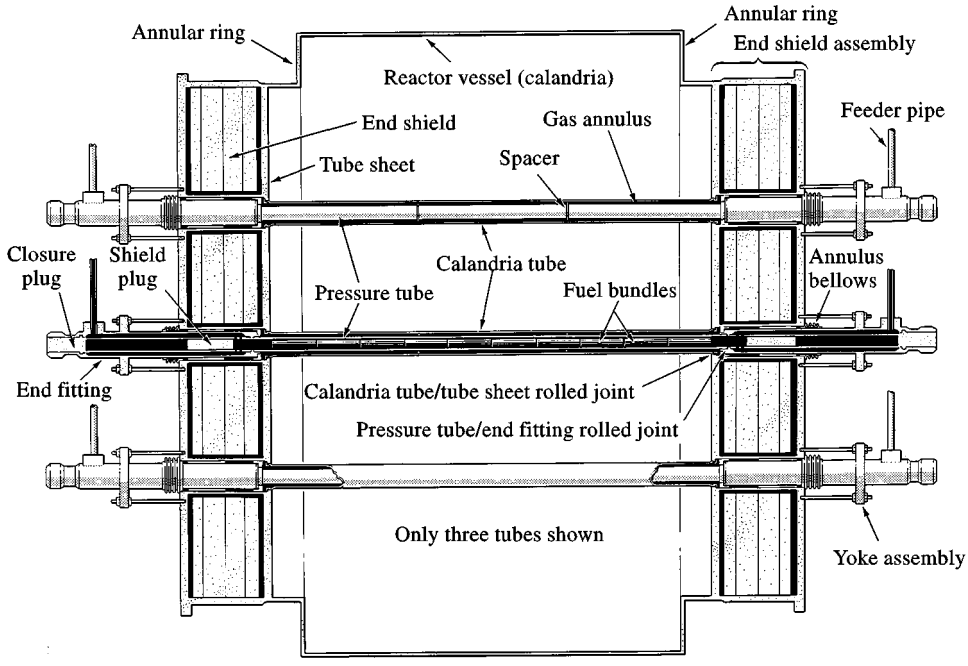

Figure 2. Simplified diagram of the CANDU reactor (not to scale).

or 13 CANDU fuel bundles rest end-to-end in each channel to form a fuel string. Heavy-water coolant enters and exits the fuel channel through the end-fittings located outside the reactor core. After entering an inlet end fitting, the coolant flows along an annular channel surrounding a linear tube, then radially inward through holes in the liner tube and the inboard end of the shield plug. A short distance downstream from the shield plug outlet the coolant enters the upstream fuel bundle. From there, the coolant flows through subchannels between the fuel elements in the fuel string, removing heat generated by the fission reaction.

Wear marks are occasionally produced in pressure tubes by the fuel bundle at the inlet end of the fuel string in the reactors of Ontario Hydro's Bruce and Darlington generating stations. These marks are the result of vibration of some of the bearing pads in contact with the pressure tube. The vibration is thought to be caused by fuel bundle motion due to both turbulence generated by the inlet fuel channel hardware, and acoustically transmitted pressure pulsations generated by the coolant pumps.

1.2. Measurement of Vibration Excitation Forces

Many researchers have examined the excitation forces due to turbulent flow acting on cylindrical structures. In general, these forces have been determined from three types of measurements: vibration response measurements; turbulent pressure measurements; and direct force measurements. In the following, work performed using each of these approaches is reviewed briefly and related to the present problem.

At Atomic Energy of Canada Limited (AECL), Pettigrew and co-workers have estimated the spectral density of the effective force per unit length acting on single flexible cylinders (i.e., fuel elements and steam-generator tubes) based on modal vibration amplitudes and modal characteristics (Pettigrew & Gorman 1981; Pettigrew & Taylor 1994). This approach assumes that the pressure field is homogeneous and that the frequency content is broad-banded relative to the cylinders frequency response. Information can only be obtained for force components at the natural frequencies of the cylinder. Using this approach, the excitation forces acting on individual fuel elements in single- and two-phase flow have been characterized. However, through dynamic interaction measurements and other means, it was demonstrated that individual fuel element vibration does not cause excessive pressure tube wear.

It is more difficult to accurately characterize fuel bundle excitation forces based on bundle vibration measurements. Because the fuel bundle has an ill-defined geometry, numerous potential contact points and loose fuel pellets, and because it can be deformed easily, fuel bundle vibration characteristics tend to be nonstationary, nonlinear and inconsistent. There is also some evidence that the inlet fuel bundle is subject to aperiodic sliding motions under certain conditions. Force measurements in the time domain are most appropriate for investigating excitation of such nonlinear structures.

It is now generally accepted that sub-critical vibrations in axial flow are excited by random time-varying pressures resulting from turbulence in the fluid and from far-field disturbances (Païdoussis 1983). Chen & Wambsganss (1970) predicated the vibration of a cylinder based on the statistical properties of the wall pressure field measured on a body of revolution by Bakewell (1968). Gorman (1971) and Ohlmer *et al.* (1972) measured cylinder vibration and statistics of the wall pressure in the annular gap around the cylinder. Taking both measurements in the same facility led to better agreement between predicted and measured cylinder vibration amplitudes. Mulcahy *et al.* (1980) showed that upstream turbulence quickly dies out once flow enters a confined annular gap around a single cylinder

and hence has little influence on the cylinder vibration amplitude. Olhmer (1973) measured the turbulent pressures on one cylinder in a three-cylinder cluster. More recently, Curling & Paidoussis (1992) have measured turbulent pressure correlations between different cylinders in a multi-cylinder cluster. While most investigators used matched pairs of miniature pressure transducers diametrically opposed in the cylinder walls [e.g., Mulcahy *et al.* (1982) and Wambsganss & Zaleski (1970)], Gorman (1971) used two differential pressure transducers each connected to the opposite sides of the exterior flow tube.

In the current investigation, it was not considered feasible to characterize the surface pressures acting on a complete fuel bundle. However, attempts were made to measure some turbulent pressure statistics on the exterior flow tube using flush-mounted pressure transducers. This attempt was relatively unsuccessful because of insufficient transducer calibration accuracy.

Instead of integrating surface pressures, Inada *et al.* (1991) used strain-gauged load fixtures to measure the turbulent forces acting on short segments of a cylinder in axial annular flow. Savkar & So (1978) measured the buffeting forces on a cylinder in cross-flow using a short stiff cylinder mounted across a wind tunnel on piezo-electric force transducers. Simonis & Johnston (1988) used a strain-gauge-based load fixture to measure unsteady lift and drag forces on cylinders in a tube array mounted across a water tunnel. Taylor *et al.* (1988) did similar work in two-phase air–water flow using piezo-electric force transducers. Unsteady forces on aerodynamic wind tunnel models are also routinely measured with load fixtures.

The CANDU fuel bundle motions of most concern are at frequencies less than about 30 Hz. These motions are characterized by almost rigid-body displacements and rotations. For example, the fundamental vibration mode involves "rocking" from side-to-side in the pressure tube. For these types of modes, the modal excitation forces can be accurately estimated from the forces and moments acting on the fuel bundle. Considering the features of the fuel bundle, the measurement of the total force and moment components was thought to be the most cost-effective way to characterize the damage potential of the turbulence generated by the inlet fuel channel hardware.

2. BUNDLE LOAD MEASUREMENT RIG

The BLM rig consists of a fuel bundle model, the "test bundle", mounted on force transducers in a segment of aluminium "pressure tube". The geometry of the test bundle was designed to accurately represent the wetted surface of a fuel bundle. The bundle model also had to be stiff and lightweight, to ensure that is fundamental natural frequencies were well above 100 Hz in order to avoid interference with turbulence force measurements.

As shown in Figures 3 and 4, the test bundle consists of two solid Zircaloy rods and 35 empty Zircaloy fuel elements welded to standard end-plates. These rods and elements are also connected at three positions along their lengths via welded spacer pads. The test bundle has a mass of only 2·98 kg, making it about 20% more dense than water.

The test bundle is supported by four, three-axis, quartz force transducers (Kistler model 9251A4) mounted in assemblies as shown in Figure 4. Transducer pairs are mounted a quarter bundle length from each end of the bundle. The transducers in each pair are preloaded against diametrically opposite sides of the bundle. Each force transducer is connected to the test bundle via an axisymmetric component (Component A in Figure 4) which fits into a shallow hole milled in the solid Zircaloy rods. Because the force transducers and transducer assemblies are very stiff, the O-ring seal between the "on-balance" and "off-balance" components (Components A and C in Figure 4) has no effect on the

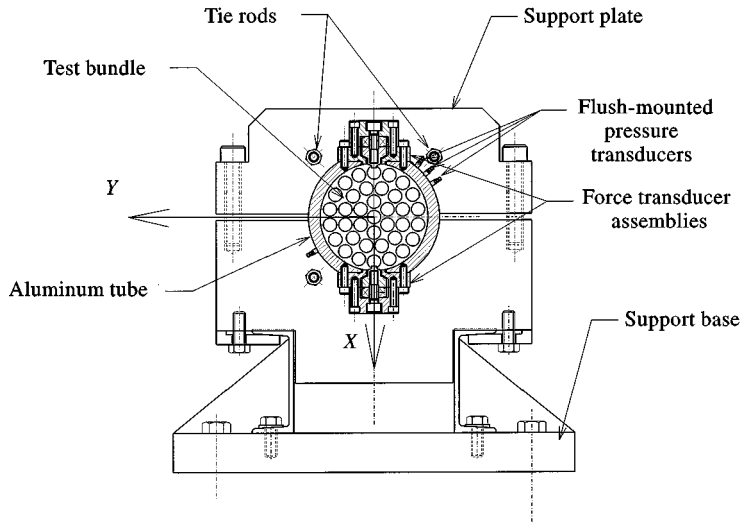

Figure 3. Cross-section through the BLM rig.

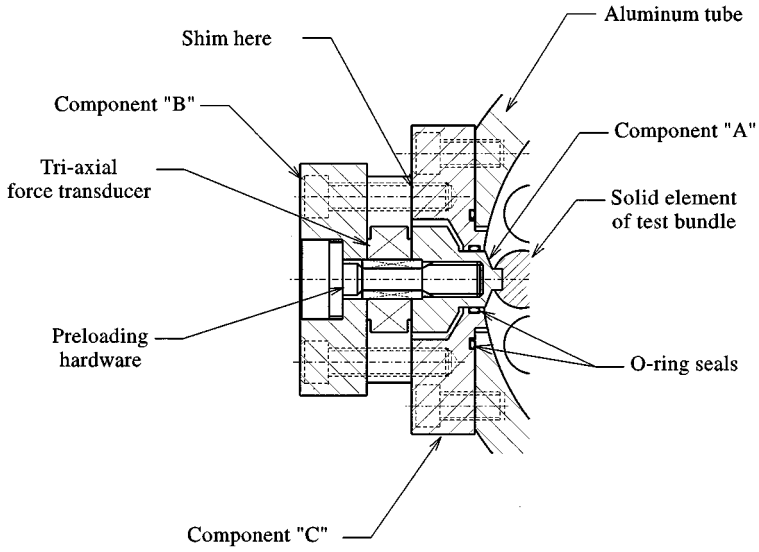

Figure 4. Cross-section through a force transducer assembly of the BLM rig.

measured loads as long as metal-to-metal contact is avoided. Adjustment of the preload and the bundle position in the X-direction is accomplished by shimming as shown in Figure 4. The position in which the force transducer assembly is clamped to the aluminium tube determines the bundle Y-position. During testing, the aluminium tube was rigidly attached to a stiff base to control test-section vibration.

Steady and dynamic loads were measured with the charge amplifiers (Kistler model 5010A12) operating in long and short time-constant modes, respectively. The accuracy of each charge amplifier is $\pm 0{\cdot}5\%$ and the force transducers have a linearity of $\pm 1\%$.

Various interchangeable acrylic tube segments were made for use upstream and downstream of the aluminium pressure tube. This arrangement allowed the clearance between the bundle model and the inlet hardware to be varied and an upstream bundle to be added.

Three orthogonal accelerometers (Kistler model 8704B100) were mounted on the test-section. Acceleration/force coherence functions were calculated to estimate the portion of each measured force that was due to the vibration of the test-section.

During each test, the 12 force and three accelerometer signals were recorded on the FM channels of a TEAC tape recorder (model XR-7000). These recorded analog signals were later played back and digitized using a high-speed data-acquisition card (Computer Boards model CIO-DAS16/330). Snap-Master™ (version 2.00c) software was used as a data-acquisition controller and for time/frequency-based analysis.

In this paper, the coordinate axes are defined with the X-axis being positive downward, the positive Z-axis in the flow direction, and the Y-axis in the lateral direction (Figure 3).

2.1. Steady Load Measurement

Static calibration tests were performed to ensure that all force transducers were installed and functioning properly and, in particular, to detect metal-to-metal contact between on- and off-balance portions of the test-rig. The calibration results were used to correct the measured steady forces for a small amount of cross-talk between the large axial drag load and the other measured load components. The calibration procedure consisted of comparing a series of known static forces to the corresponding measured forces and moments. Factors relating the measured load components to the applied force were calculated by linear regression and assembled into a calibration matrix. The inverse of this calibration matrix was then used to correct the measured loads.

Steady bundle loads were measured by taking the difference between the average loads at a given flow rate and the average loads after the flow had been shut off. The force signals were recorded over a period from 60 s before to 60 s after the flow control valve was closed. The data-acquisition software was used to digitally sample the 12 force transducer signals and combine these to calculate the three forces and three moments acting on the test-bundle. A series of 5 s averages of the total forces and moments was written to a computer file for further analysis. The steady forces were calculated by measuring the magnitude of the step that occurred in the averaged signals. The correction based on static calibration measurements was then applied.

The steady loads on the bundle were measured with the charge amplifiers operating in a long time-constant mode. This mode allowed the forces to be measured over a period of several minutes without significant signal loss. The output of the charge amplifers did exhibit a drift rate that was constant over a single test. The measured forces were corrected based on the observed drift rate.

Repeat flow tests indicated that the measured X- and Y-forces were repeatable within $\pm 0{\cdot}6\%$ and $\pm 0{\cdot}2\%$ of the axial load, respectively. The O-ring seals between the on- and off-balance portions of the force transducer assemblies are thought to account for much of the variability in the steady force measurements. Unbalanced residual forces probably result from deformations of the rubber due to the pressure changes that accompany flow rate changes.

2.2. Unsteady Load Measurement

Measurement of unsteady forces was accomplished with the force transducer charge amplifiers operating in a short time-constant mode. Once a selected condition had been established, the 12 force signals (4 transducers, and 3 forces per transducer) and the three accelerometer signals were recorded simultaneously. These recorded signals were later digitally sampled at a rate of 1024 samples per second. The signals were used to calculate the instantaneous total forces and moments acting about the centre of the test bundle. The instantaneous X-force and Y-moment were used to calculate a pair of equivalent X-forces acting at either end of the bundle, F_{x1} and F_{x2}. Similarly, instantaneous equivalent end forces in the Y-direction, F_{y1} and F_{y2}, were determined from the Y-force and X-moment. These bundle "end forces" provide a convenient way of examining the distribution of the transverse hydrodynamic forces along the length of the bundle. Instrument noise limited the resolution of the dynamic loads to about 0.02 N.

Dynamic calibration tests of the test bundle were performed to determine frequency response functions relating the applied force or moment to the measured forces and moments. Realistic damping and mass characteristics were obtained by performing the calibration of the test bundle while it was completely immersed in quiescent water inside the pressure tube. Nine different dynamic calibration tests were done using mechanical shakers to apply random forces. A single shaker was employed to apply an axial force (F_Z) and end forces (F_{x1}, F_{x2}, F_{y1}, and F_{y2}). Two shakers, one attached to either end of the test bundle, were used to apply the remaining loads. Pure forces, F_x and F_y, were applied by driving the shakers in-phase, while moments, M_x and M_y, were applied by driving the shakers 180° out-of-phase. The shakers were driven with white noise, low-pass filtered at 300 Hz.

Gain factors for the bundle forces and moments are shown in Figure 5. The gain factor in the axial direction is approximately 1 for frequencies up to over 300 Hz. In contrast, the gain

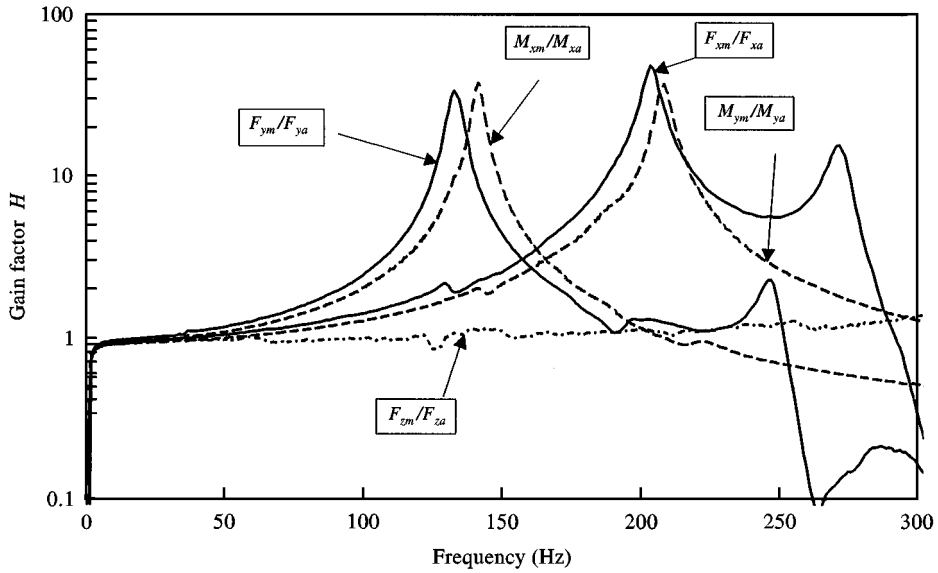

Figure 5. Gain factors for forces and moments measured in the calibration testing of the BLM rig.

factors of the transverse forces and moments show large peaks at the first and second natural frequencies of the test bundle. The lowest natural frequencies of the test bundle are at about 135 Hz in the Y-direction and 205 Hz in the X-direction. The gain factors vary between 0·8 and 1·4 in the frequency range from 3 to 70 Hz. Although flow-related damping is expected to reduce the gain factors near the resonant frequencies, it should have little effect below 70 Hz. The gain factor below 3 Hz is significantly reduced due to the limited response of the charge amplifiers in the short time-constant mode at these low frequencies. The coherence between the applied and measured loads is greater than 0.98 throughout the frequency range tested.

The gain factors between an applied load and its orthogonal load components were all quite small. Since the unsteady force components were of about the same magnitude, there was no need to correct for cross-talk.

One-sided power spectral densities (PSDs) were calculated from the forces, moments, and end forces caused by turbulence in the coolant flow. Average PSDs were calculated from 50 1-s, nonoverlapping samples. The corresponding 95% confidence interval on a single-frequency component of the average PSD is $\pm$ 28%. In tests performed after those reported in this paper, the average PSDs were determined from 300 1-s samples to reduce the confidence interval to $\pm$ 12%. The average PSDs were corrected by dividing by the square of the appropriate gain factor (magnitude of the frequency response function), determined from the dynamic calibration tests.

Root-mean-square (r.m.s.) values of the unsteady loads were calculated from the corrected PSDs using

$$F_{\text{rms}} = \sqrt{\int_{f_1}^{f_2} S_{FF}(f)\,\mathrm{d}f}, \tag{1}$$

where F_{rms} is the r.m.s. force, S_{FF} is the force PSD, f is the frequency, and f_1 and f_2 are the upper and lower bounds of the frequency band to be included in the r.m.s. force. R.m.s. values displayed in this paper are for a band from 3 to 70 Hz.

3. LOOP TEST FACILITIES

Testing was performed both in the flow visualization loop at AECL's Sheridan Park Engineering Laboratory (SPEL) and in a flow loop at AECL's Chalk River Laboratories (CRL). Figure 6 is a photograph of the BLM rig installed at SPEL. In both loops, pumps provide a flow of room temperature water to the test-section at rates up to 32.5 kg/s. The test-section components were mounted on an I-beam supported on steel posts at SPEL and on a heavy steel pedestal attached to the concrete floor at CRL. At SPEL, the use of a reinforced rubber pipe to connect the pump was expected to prevent the transmission of vibration to the test-section and, because of the acoustic impedance mismatch, to reduce the transmission of far-field noise.

Acceleration measurements taken on the BLM rig during testing were used to quantify the effect of the test-section vibration on the measured bundle forces. Coherence functions between the measured forces and accelerations showed that a very small fraction of the loads on the test-bundle were generated by the test-section motion. This confirmed that the loads measured with the BLM rig were almost exclusively due to the hydrodynamic forces to the coolant flow.

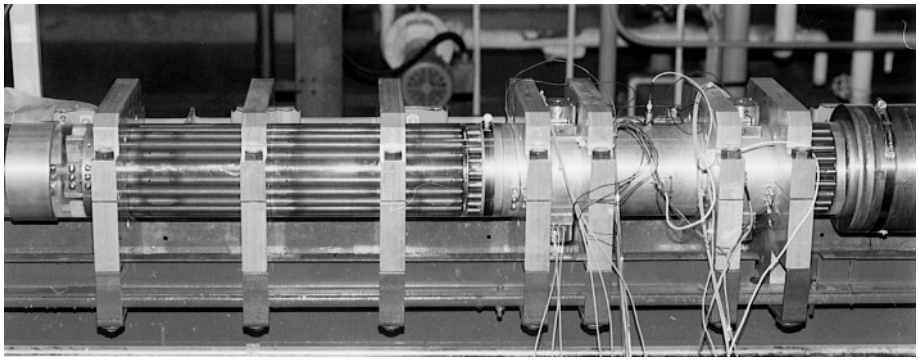

Figure 6. Photograph of the BLM rig installed in the SPEL flow visualization loop.

4. TEST PROGRAM

One of the more important tasks performed with the BLM rig was the comparison of coolant forces associated with the original Bruce/Darlington inlet shield plug, Mk 3A, and various modified shield plugs. An inlet shield plug is located in each inlet end fitting and permits the coolant flow to enter the channel while acting as a radiation shield. Figure 7 shows photographs of the downstream end of two types of these shield plugs. The Mk 3A has four circular flow passages with streamlined entrances and exits, as shown in Figure 7(a). The Mk 3C design was developed during the Bruce/Darlington shield plug redesign program (Field *et al*. 1996). This shield plug is identical to the Mk 3A except for the addition of a flow straightener at the outlet of the shield plug as shown in Figure 7(b). This flow straightener consists of a 42 mm thick plate with a large number of 6.4 mm diameter holes bored through it.

In addition to examining the effect of inlet fuel channel hardware, the BLM rig was used to study the effects of upstream orifice plates, a downstream bundle, an upstream bundle, bundle-to-shield-plug clearance distance, bundle position within the pressure tube, acoustic excitation forces, bundle orientation and end-fitting orientation. During most tests, the test

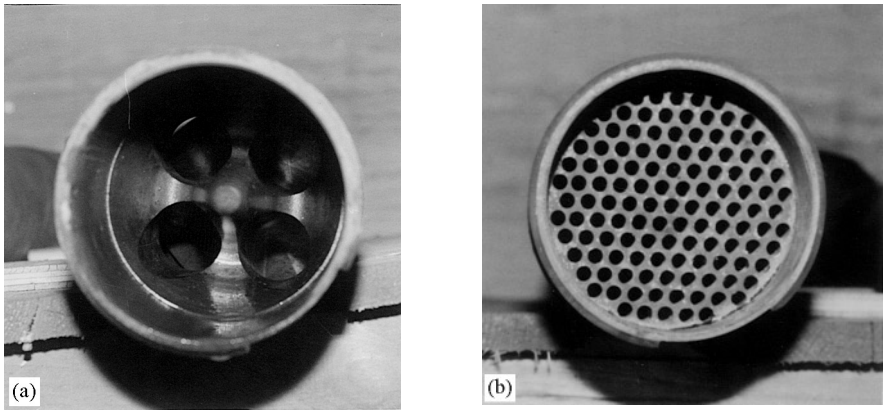

Figure 7. Photographs of downstream ends of shield plugs: (a) end view of Mk 3A; (b) end view of Mk 3C.

bundle was located in an eccentric configuration that closely approximated the position of a fuel bundle resting on the bottom of the pressure tube. Measurements were taken over a range of flow rates up to 32·5 kg/s. It was found necessary to fix a fuel bundle downstream of the test bundle, as shown in Figure 6, to avoid wake shedding forces on the downstream end of the test bundle. A gap of between 1 and 3 mm was maintained between the bundles in order to eliminate any direct force transmission.

5. RESULTS AND DISCUSSION

5.1. Steady Forces

Table 1 lists the measured steady loads and their corresponding dimensionless coefficients as a function of the average flow velocity in the bundle model with the Mk 3A and Mk 3C shield plugs. The table also shows the Reynolds number based on this average velocity, U_b, and the diameter of the bundle, D, defined as

$$\mathrm{Re} = \frac{\rho U_b D}{\mu}, \tag{2}$$

where ρ and μ are the density and viscosity of the fluid, respectively. The force coefficients, C_F, were determined by normalizing the force, F, by the product of the dynamic pressure in the bundle, $q = 1/2\rho U_b^2$ and an effective area (LD),

$$C_F = \frac{F}{\frac{1}{2}\rho U_b^2 LD}, \tag{3}$$

where L is the length of the bundle.

The Mk 3A shield plug resulted in X-direction transverse forces (negative lift) on the test bundle that were about two to three times greater than those produced with the Mk 3C shield plug. The side forces were both close to zero. None of the transverse force coefficients showed a statistically significant trend with Reynolds number. Tests with another shield plug were performed with the test-section in three different orientations. These tests showed that about two-thirds of the transverse force rotated with the bundle model and the

Table 1
Steady forces with Mk 3A and Mk 3C shield plugs

Shield plug	Flow velocity (m/s)	Reynolds number (millions)	F_x (N)	F_y (N)	F_z (N)	C_{F_x}	C_{F_y}	C_{F_z}
MK 3A	2·9	0·33	2·7	− 0·9	113	0·013	− 0·004	0·54
	5·8	0·65	8·0	− 1·4	415	0·010	− 0·002	0·49
	5·8	0·65	7·7	− 2·3	419	0·009	− 0·003	0·49
	7·7	0·87	14·0	− 1·3	723	0·009	− 0·001	0·48
	9·3	1·05	21·9	2·4	1015	0·010	0·001	0·46
MK 3C	3·0	0·34	1·6	− 0·4	121	0·007	− 0·002	0·54
	5·8	0·66	4·4	− 0·3	431	0·005	− 0·000	0·50
	5·8	0·66	4·3	− 1·6	414	0·005	− 0·002	0·48
	7·8	0·88	7·4	1·0	717	0·005	0·001	0·47
	9·1	1·03	6·8	1·8	992	0·003	0·001	0·47

remaining third was fixed with respect to the end-fitting. Earlier tests had shown that the small eccentricity of the test bundle with respect to the pressure tube did not have a significant effect on the transverse forces or moments when the upstream field was undisturbed. The X and Y moments (not shown) were consistent with the transverse forces being applied near the upstream end of the bundle.

The steady transverse forces are important because they can affect the dynamic support stiffness of the fuel bundle and the contact forces between the fuel bundle and the pressure tube. For instance, a lift force applied near the upstream end of the inlet fuel bundle will tend to reduce the number of bearing pads in contact with the pressure tube, decreasing the support stiffness and lowering the bundle rocking mode frequency. This lift force also increases the possibility that the unsteady forces will be able to overcome friction and cause the inlet end of the bundle to shift periodically.

The axial force and drag coefficients associated with both shield plugs are very similar. In both cases, a gradual reduction in drag coefficient with increasing Reynolds number is observed.

5.2. Unsteady Transverse Forces

Figure 8 presents the r.m.s. values of the unsteady side and vertical forces measured with the Mk 3A and Mk 3C shield plugs as a function of the average flow velocity in the bundle. With the Mk 3A shield plug, the r.m.s. side force is twice as large as the r.m.s. vertical force. The r.m.s. side and vertical forces with the Mk 3C are practically identical, being about 25% of the side-force with the Mk 3A. The forces measured with the Mk 3C shield plug are very similar to those measured downstream of a fuel bundle and lower than those measured at the end of a long straight pipe. It therefore appears that further shield plug modifications are unlikely to result in significantly lower unsteady forces than those due to the Mk 3C shield plug.

Figure 9 is a graph of dimensionless PSDs of the side-forces plotted against the reduced frequency, $f_r (= fD/U_b)$, for the Mk 3A and the Mk 3C shield plugs. The dimensionless force

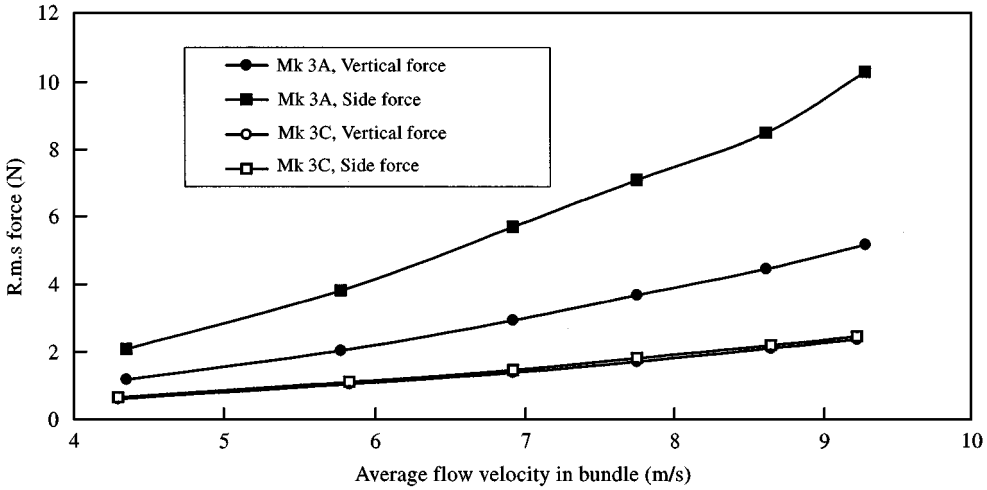

Figure 8. R.m.s. side and vertical forces measured with Mk 3A and Mk 3C shield plugs.

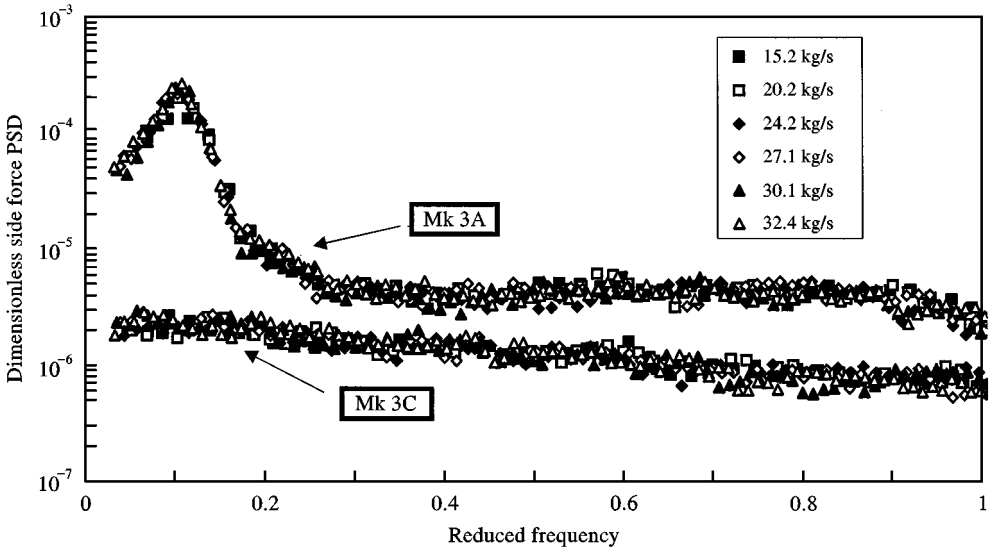

Figure 9. Dimensionless PSDs of upstream end side force for Mk 3A and Mk 3C shield plugs.

PSD, $\tilde{S}_{FF}$, was defined as follows:

$$\tilde{S}_{FF} = \frac{S_{FF}U_b}{(qLD)^2 D} = \frac{4S_{FF}}{\rho^2 L^2 D^3 U_b^3}, \tag{4}$$

where S_{FF} is the force PSD, U_b is the average fluid velocity through the bundle, ρ is the fluid density, L is the bundle length, and D is the bundle diameter. This dimensionless PSD was determined by normalizing the forces using the dynamic pressure times a representative area (LD) and normalizing the frequency by U_b/D. Note that, in Figure 9, the results for all flow rates fall within a band that varies by less than a factor of two from its lower to its upper bound. This variation is consistent with the confidence interval of the PSDs and confirms that test-section vibration and acoustically transmitted far-field noise have not significantly affected the unsteady transverse force measurements. It also illustrates that Reynolds number has a relatively small effect on these unsteady forces. Au-Yang *et al.* (1994) also found that the Reynolds number had little effect on the turbulent pressures measured between the reactor vessel and core support cylinders of a pressurized water reactor.

With the Mk 3A shield plug, the r.m.s. upstream end forces were about 160% higher than the corresponding downstream end forces. This indicates that most of the unsteady transverse forces are applied near the upstream end of the bundle. With the Mk 3C shield plug or a fuel bundle upstream, the upstream end forces were only 30 to 70% higher than the corresponding downstream end forces indicating that the turbulent forces act more uniformly along the length of the test bundle.

In Figure 9, the Mk 3A shield plug side-force consistently shows a peak at a reduced frequency of 0·11. This peak is caused by a vortex-shedding-like flow instability within the liner tube. The corresponding PSD of the vertical force (not shown) is very similar, except that the peak is greatly reduced. This accounts for the smaller r.m.s. vertical force shown in Figure 8. Other tests showed that the direction in which the forces caused by the flow instability act is determined by both the bundle and end-fitting orientations, as is the case with the steady forces.

Compared to the Mk 3A, the Mk 3C shield plug eliminates the force peak due to the flow instability and reduces the broad-band force level. The flow straightener in the Mk 3C shield plug apparently acts to eliminate the momentum fluctuations due to the flow instability and to reduce the scale of the turbulence and hence the broad-band excitation. The force spectra obtained with the Mk 3C shield plug are very similar to those obtained with a fuel bundle upstream from the test bundle.

6. CONCLUSIONS

The BLM rig was used to accurately measure the hydrodynamic forces on a CANDU fuel bundle at room temperature. The results presented illustrate how the bundle excitation forces are affected by the upstream hardware, and in particular, how the steady and unsteady transverse forces are significantly reduced with the addition of a flow straightener to the original shield plug design. Dimensionless force PSDs measured at different flow rates can be collapsed onto a single curve that may be used to predict the bundle excitation forces at reactor conditions.

Before the development of the BLM rig, comparisons between shield plugs were based primarily on fuel bundle vibration measurements and pressure tube wear damage. Because of the nonstationary and highly variable nature of the dynamic response characteristics of fuel bundles and the variety of factors that can affect this response, a great many tests at reactor conditions were often required to establish the effect of modifications to the inlet hardware. In spite of all these tests, there was no clear understanding of how the steady and unsteady forces acting on the bundle changed to produce observed differences in vibration. The BLM rig can now be used to measure these forces directly in a single test at room temperature. This load measuring technique has shown itself to be ideal for assessing the damage potential of different fuel channel inlet hardware designs.

ACKNOWLEDGEMENTS

This work was funded by the CANDU Owners Group: Process Systems and Equipment (TC # 1) under work package WPIR 0137. The authors would like to thank M. J. Pettigrew for his support and advice during the course of this work. The authors would also like to thank P. Adams, J. H. Tromp, K. M. Boucher, and E. O. McKerrow at Chalk River Laboratories for their effort in the design, construction and operation of the BLM rig. The assistance of K. Saari, B. Burgess, and K. Cheatle at SPEL was greatly appreciated.

References

Au-Yang, M. K., Brenneman, B. & Raj, D. 1994 Flow-induced vibration test of an advanced water reactor model: Part 1 — turbulence induced forcing function. In *Flow-Induced Vibration* 1994 (ed. M. K. Au-Yang), PVP-Vol.273, pp. 43–65. New York: ASME.

Bakewell, H. P. 1968 Turbulent wall-pressure fluctuations on a body of revolution. *Journal of the Acoustical Society of America*, **43,** 1358–1363.

Chen, S. S. & Wambsganss, M. W. 1970 Response of a flexible rod to near-field flow noise. *Proceedings of the conference on Flow-Induced Vibrations in Reactor System Components*, ANL-7685, pp. 5–31.

Curling, L. R. & Païdoussis, M. P. 1992 Measurements and characterization of wall-pressure fluctuations on cylinders in a bundle in turbulent axial flow; Part 1: Spectral characteristics, and Part 2: temporal characteristics. *Journal of Sound and Vibration* **157,** 405–433.

Field, G. J., Smith, B. A. W. & Tse, K. 1996 Development of a flow straightening inlet shield plug. *Proceedings of ASME-PVP Symposium on Flow-Induced Vibration*, Montreal, pp. 173–182.

GORMAN, D. J. 1971 An analytical and experimental investigation of the vibration of cylindrical reactor fuel elements in two phases parallel flow. *Nuclear Science and Engineering*, **44,** 277–390.
INADA, F., KAWAMURA, K. & YASUO, A. 1991. A study of random fluid forces acting on a tube in parallel two-phase flow. *Proceedings of I. Mech. E. International Conference on Flow Induced Vibrations*, Paper C416/032, pp. 379–384.
MULCAHY, T. M., LAWRENCE, W. & WAMBSGANSS, M. W. 1982 Dynamic surface-pressure instrumentation of rods in parallel flow. *Journal of Experimental Mechanics*, **22,** 31–36.
MULCAHY, T. M., YEH, T. T. & MISKEVICS, A. J. 1980 Turbulence and rod vibrations in an annular region with upstream disturbances. *Journal of Sound and Vibration*, **69,** 59–69.
OHLMER, E. 1973 Experimental investigation of an analytical model for parallel flow induced vibrations of rod structures. *Proceedings of the International Symposium on Vibration Problems in Industry*, Keswick, U.K., pp. 1–20.
OHLMER, E., RUSSO, S. & SCHWEMMLE, R. 1972 Investigation of an analytical model for parallel flow induced rod vibrations. *Nuclear Engineering and Design*, **22,** 272–289.
PAÏDOUSSIS, M. P. 1983 A review of flow-induced vibrations in reactors and reactor components. *Nuclear Engineering and Design*, **74,** 31–60.
PETTIGREW, M. J. & GORMAN, D. J. 1981 Vibration of heat exchanger tube bundles in liquid and two-phase cross-flow. In *Flow-induced Vibration Design Guidelines*, PVP-Vol.52, pp. 89–110; also, AECL Report AECL-7264.
PETTIGREW, M. J. & TAYLOR, C. E. 1994 Two-phase flow-induced vibration: an overview. *ASME Journal of Pressure Vessel Technology*, **116,** 233-253.
SAVKAR, S. D. & SO, R. M. C. 1978 Buffeting in single cylinders. *Proceedings of the Keswick International Conference on Vibration in Nuclear Plant*, pp. 189–204.
SIMONIS, J. C. & JOHNSTON, J. E. 1988 Experimental determination of turbulent buffeting effects in tube bundles. In *Proceedings ASME International Symposium on Flow-Induced Vibration and Noise*; *ASME Flow-Induced Vibration in Heat-transfer Equipment* (eds. M. P. Païdoussis *et al.*) New York: Vol. 5, pp. 65–85.
TAYLOR, C. E., PETTIGREW, M. J., Axisa, F. & VILLARD, B. 1988 Experimental determination of single and two-phase flow induced vibration forces on tube rows. *ASME Journal of Pressure Vessel Technology*, **110,** 22–28.
WAMBSGANSS, M. W. & ZALESKI, P. L. 1970 Measurement interpreation and characterization of nearfield flow noise. *Proceedings of the Conference on Flow-induced Vibrations in Reactor System Components*, ANL-7685, pp. 112–140.

APPENDIX: NOMENCLATURE

C_{F_x}	dimensionless X-force, $F_x/(LDq)$
C_{F_y}	dimensionless Y-force, $F_y/(LDq)$
C_{F_z}	dimensionless Z-force, $F_z/(LDq)$
D	nominal bundle diameter
F	force
L	bundle length
Re	Reynolds number, $\rho U_b D/\mu$
S_{FF}	one-sided power spectral density of force
$\tilde{S}_{FF}$	dimensionless one-sided power spectral density of force
U_b	average fluid velocity through the bundle
X	X-coordinate (X-axis origin at the bundle centre, positive is downward)
Y	Y-coordinate (Y-axis origin at the bundle centre, positive is to the right when facing upstream)
Z	Z-coordinate (Z-axis origin at the bundle centre, positive in the flow direction)
M	moment

f	frequency
f_r	reduced frequency, fD/U_b
q	dynamic pressure, $\rho U_b^2/2$
μ	Absolute viscosity
ρ	fluid density

Subscripts

a	refers to applied force
m	refers to measured force
rms	root-mean square
x	X-direction
x_1	X-direction at upstream end
x_2	X-direction at downstream end
y	Y-direction
y_1	Y-direction at upstream end
y_2	Y-direction at downstream end
z	Z-direction